ChemComm

COMMUNICATION

View Article Online
View Journal | View Issue

Cite this: *Chem. Commun.*, 2025, **61**, 17850

Received 24th July 2025,
Accepted 9th October 2025

DOI: 10.1039/d5cc04069h

rsc.li/chemcomm

Spectroscopic characterisation of metastable photoswitches for CO_2 capture and release

Federico J. Hernández *[a] and Basile F. E. Curchod *[b]

The design of functional molecules for seawater CO_2 capture *via* photoisomerisation offers a less energy-intensive approach for atmospheric CO_2 depletion, yet requiring efficient photon absorption at wavelengths matching the solar irradiance spectrum. Computational photochemistry can predict absorption spectra, reducing reliance on trial-and-error experiments. However, guiding principles for reliably describing the shape and absolute intensity of absorption spectra are lacking. Herein, we present a simple protocol for calculating absorption spectra of photoacids in solution with quantitative accuracy. This approach enables predictive modelling of photoactive systems and is readily transferable to other solar-driven technologies based on functional molecules.

The presence of atmospheric CO_2, necessary for life on Earth yet a main driver of anthropogenic climate change, must be reduced urgently to avoid catastrophic environmental consequences.[1,2] While the use of photoactive molecular materials for direct air capture technologies is advancing,[3,4] the idea of CO_2 removal from seawater has recently gained attention as a scalable and sustainable alternative.[5–10] Seawater absorbs about 25% of anthropogenic CO_2 emissions and contains nearly 130 times more CO_2 per unit volume than does air, primarily in the form of bicarbonate.[11] Considering the equilibrium $CO_2(g) \rightleftharpoons CO_2(aq)$ at the oceanic surface, the CO_2 concentration in seawater increases proportionally to the increase in CO_2 in the atmosphere.[11] Hence, the sustained extraction of CO_2 from seawater indirectly enhances atmospheric drawdown. In this context, photochemical systems that enable CO_2 capture and release *via* light activation offer a promising route to negative emissions without requiring thermal energy or complex infrastructure. Visible-light-responsive molecular systems, particularly those based on photoacids (molecules that release protons upon absorbing light), could enable decentralised and energy-efficient carbon capture platforms aligned with solar cycles.[5–8]

Metastable-state photoacids,[12] such as the well-known merocyanine (MC)/spiropyran (SP) pair, have emerged as particularly appealing for light-induced CO_2 capture and release (Scheme 1). Upon irradiation, the protonated merocyanine (MCH^+) releases a proton and cyclises to yield a neutral spiropyran, generating large, reversible pH swings.[5–8] These photoinduced protonation changes have been used to modulate carbonate equilibria in aqueous and DMSO/water media, enabling reversible CO_2 capture and release.[5–8] The molecular design of the MC/SP pair features tunable acidity, polarity, and spectral properties, making it a versatile platform for developing light-driven separations.

A key aspect of photoacid-based CO_2 capture and release technologies is the efficient photoisomerisation triggered by solar irradiation. While this technology can formally operate at no external energy cost, the molecular design must ensure that MCH^+ species absorb light efficiently in the visible and near-UV spectral regions to enable efficient photoisomerisation. Hence, the design of next generations of photoacids for CO_2 capture and release relies on quantitative predictions of their absorption spectrum. More specifically, predictions should not focus solely on the absorption maxima but rather on the overall shape of the absorption spectrum (as a function of wavelength, λ) as well as its absolute intensity (molar extinction coefficient, $\varepsilon(\lambda)$), key ingredients to enhance the rate of photoisomerisation. Such considerations imply that single-point calculations, commonly used in computational photochemistry to characterise the

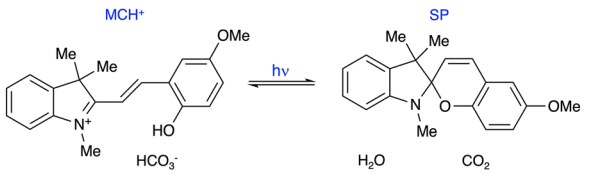

Scheme 1 Photoisomerisation of the protonated merocyanine (MCH^+) to spiropyran (SP) and its application to seawater CO_2 capture and release.

[a] *Department of Chemistry, Queen Mary University of London, Mile End Road, London E1 4NS, UK. E-mail: f.hernandez@qmul.ac.uk*
[b] *Centre for Computational Chemistry, School of Chemistry, University of Bristol, Bristol BS8 1TS, UK. E-mail: basile.curchod@bristol.ac.uk*

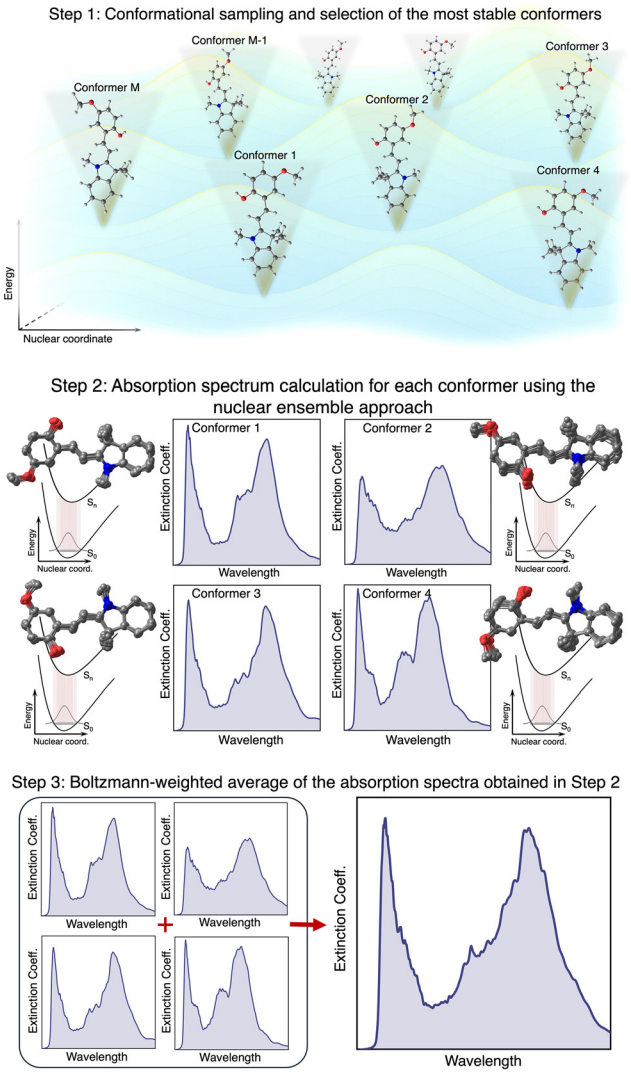

Fig. 1 Schematic of the computational protocol proposed to calculate absorption spectra of complex molecules, illustrated using MCH^+. Hydrogen atoms are omitted in step 2 for clarity.

vertical excitations of a molecule, are insufficient to predict future photoacids for CO_2 capture and release. Building upon recent works in atmospheric photochemistry,[13,14] we introduce in the following a simple and practical computational protocol to quantitatively simulate the absorption spectra ($\varepsilon(\lambda)$) of photoacids (and other complex molecules) in solution.

The protocol proposed in this work is summarised in Fig. 1. A brief overview of the protocol steps is provided here; full details are available in Section S1 of the SI. Step 1: identify all the molecular conformers present at a given temperature. For this, we perform a conformational search ensuring a thorough sampling of the ground-state potential surface of the molecule using a meta-dynamics driven search algorithm followed by geometry optimisations. This step requires an electronic-structure method with a reasonable cost-to-accuracy ratio. We used the implementation in the Crest v2.11.2 software package with the semiempirical tight-binding method GFN2-xTB.[15,16] Once all conformers are located, a second optimisation step followed by normal-mode calculations with an electronic-structure method of higher accuracy, *e.g.*, density functional theory (DFT) or MP2, is performed. In our work, we used DFT with the CAM-B3LYP[17] functional along with the conductor-like polarisable continuum model (CPCM)[18] with the electrostatic parameters of DMSO (ε = 47.2) to represent the electrostatic environment of the solvent, and the Pople basis set 6-311++G(d,p)[19] as implemented in the Orca v5.0.4 software package.[20] The relative Boltzmann population of each conformer i, p_i, is calculated using the Gibbs free energies within the harmonic approximation: $p_i = e^{-\Delta G_i \beta} \Big/ \sum_j^M e^{-\Delta G_j \beta}$, with $\beta = \frac{1}{k_B T}$, k_B is the Boltzmann constant, and M the total number of conformers. This analysis is used to decide which conformers will be considered for the next steps (see Section S2 in the SI for a detailed discussion). Step 2: calculate the absorption spectrum for each conformer selected. The nuclear ensemble approach (NEA) is used for this step as it allows to approximate the shape and intensity of an absorption spectrum and includes non-Condon effects.[14,21,22] This technique approximates the ground-state distribution of a molecule and samples from it a set of molecular geometries used to predict the absorption spectrum. In the current protocol, the ground-state distribution is built from a harmonic Wigner distribution, from which N_p different molecular configurations are sampled for each selected conformer. $\varepsilon(\lambda)$ can be obtained from the excitation energies and transition dipole moments calculated for each sampled geometry and the refractive index of the medium (see ref. 21 for a detailed explanation). This step uses the implementation of the NEA within the NewtonX platform,[23] coupled with linear-response time-dependent DFT (LR-TDDFT) with the same functional and basis set as earlier, namely LR-TDDFT/CAM-B3LYP/6-311++G(d,p)/CPCM. Step 3: combine the absorption spectrum for each conformer, each weighted by its Boltzmann factor, to produce the final absorption spectrum.

The proposed protocol was deployed to simulate the absorption spectrum in DMSO of the MCH^+ compound shown in Scheme 1 (see section S2 in the SI for a discussion on the conformers selected). We begin by assessing how conformers and ground-state distribution affect the final absorption spectrum of MCH^+. Fig. 2b compares the spectrum of conformer 1 (violet dashed curve) with that of all six conformers, weighted by Boltzmann factors, using only their ground-state optimised geometries. We note that we applied an energy shift $\Delta E = -0.30$ eV to the simulated bands before converting the energy axis to wavelength. This analysis reveals that the first two absorption bands of the experimental spectrum ($\sim$360 and $\sim$460 nm) appear to be dominated by the first two electronic transitions, $S_0 \rightarrow S_1$ and $S_0 \rightarrow S_2$, both of $\pi\pi^*$ nature (see natural transition orbitals (NTOs) in Fig. 2b). Yet, this computational analysis is not recommended for predictive purposes, as the calculated spectra do not reproduce (i) the shape of the experimental bands, (ii) their absolute intensity $\varepsilon(\lambda)$, and (iii) their absorption wavelength. Step 2 of our protocol will lead to a substantial improvement over these points.

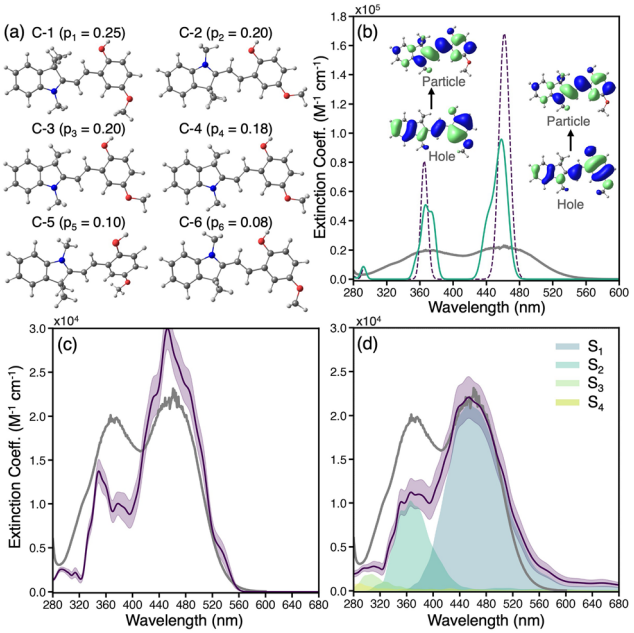

Fig. 2 Absorption spectrum of MCH^+. (a) The six different conformers of the MCH^+ derivative identified for the determination of the absorption spectrum, with their relative Boltzmann populations p_i. Conformers 2 and 3 are structurally similar (see Fig. S2 in SI for details). The total population adds to 1.01 due to rounding. (b) Molar extinction coefficients $\varepsilon(\lambda)$ from single-point calculations for the dominant conformer 1 (violet dashed curve) and an ensemble of the six conformers weighted by their Boltzmann populations (green curve). The experimental absorption spectrum measured in a 1 : 1 mixture of DMSO : water (gray curve), obtained from the authors of ref. 5, is included for comparison. An energy shift $\Delta E = -0.30$ eV is applied to the simulated transitions before transforming the energy axis to wavelength. The natural transition orbitals of the first two transitions are also included for conformer 1. (c) Absorption spectrum simulated using the NEA (violet curve) for conformer 1 and (d) for the six conformers weighted by their Boltzmann populations, compared to the experimental spectrum (grey curve). The coloured bands in panel (d) indicate the transitions to the lowest four excited states. Energy shifts $\Delta E = -0.18$ eV were applied for the spectra in panels (c) and (d) respectively. The shaded region around the main calculated absorption spectrum represents the error in $\varepsilon(\lambda)$ due to statistical sampling, as detailed in ref. 21. In all cases, a Gaussian broadening factor of $\sigma = 0.075$ eV was applied.

The absorption spectrum obtained with the NEA for conformer 1 (Fig. 2c) shows a marked improvement over the spectrum based on single-point calculations: $\varepsilon(\lambda)$ now aligns with experiment, the required energy correction drops to -0.18 eV, and the shape of the low-energy band mimics the experimental one. This improvement in the low-energy band is particularly important given that it is the one targeted to trigger CO_2 release *via* photoisomerisation under solar irradiation.[5] The simulated absorption spectrum is further improved when the six low-energy conformers of MCH^+, weighted by their Boltzmann factors (step 3 in Fig. 1), are considered (Fig. 2d). The first absorption band of this final spectrum shows a quantitative agreement with the experiment (within the statistical error of the NEA). The low-energy absorption band ($\sim$460 nm) is dominated by the $S_0 \rightarrow S_1$ transition of $\pi\pi^*$ character, whereas the high-energy absorption band ($\sim$360 nm) is dominated by the $S_0 \rightarrow S_2$ transition with a small contribution of $S_0 \rightarrow S_3$ and $S_0 \rightarrow S_4$. A natural population analysis also shows that these transitions have a small charge-transfer character (see Table S1 in SI). The lack of intensity of the calculated high-energy absorption band ($\sim$360 nm) can be related to the sampling of the low-frequency modes of the molecule (see Fig. S7 in SI).

To test our protocol further, we calculated the absorption spectrum of the related SP molecule, *i.e.*, the photoproduct of the MCH^+ photoisomerisation (Scheme 1), and compared it to experiment (Fig. 3). Four different conformers (Fig. 3a) were considered out of the 9 conformers obtained in the conformational sampling (Fig. S3a). Despite the evident difference in electronic structure between SP and MCH^+, a good agreement with experiment is again achieved for the predicted absorption spectrum (Fig. 3b). The low-energy absorption band is dominated by transitions to S_1 and S_2, whereas the high-energy band is formed by the combination of transitions up to S_3. The NTOs and the natural population analysis reveal that the main transitions have a $\pi\pi^*$ character combined with a charge-transfer contribution (in particular for the transition to S_3, see Fig. 3b and Table S1 in SI).

This improvement offered by the proposed protocol emanates, first, from the ability of the NEA to capture non-Condon effects, that is, the dependence of the electronic transition dipole moments on the nuclear geometry.[14,21,22] Non-Condon effects are here captured by sampling a large number of molecular geometries away from the equilibrium geometry. Another central ingredient is the inclusion of the main conformers present at a selected temperature in the determination of absorption spectra (compare Fig. 2c and d). Yet, a noticeable deviation between the theoretical and experimental spectra is observed for the long-wavelength tail (see Fig. 2d and 3b). This discrepancy is a result of the approximations underlying the NEA, in particular its lack of description of overlaps between

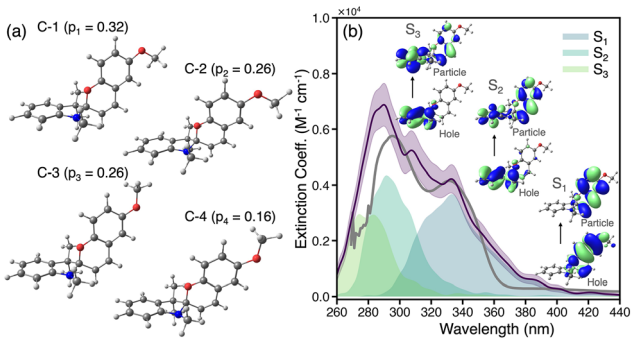

Fig. 3 Absorption spectrum of SP. (a) The four different conformers of the SP derivative identified for the determination of the absorption spectrum, with their relative Boltzmann populations p_i. (b) Absorption spectrum calculated with the NEA (violet curve) for the four conformers weighted by their respective Boltzmann population, compared to the experimental spectrum obtained from the authors of ref. 5 (grey curve). The coloured bands in panel (b) indicate the transitions to the lowest three excited states. $\Delta E = -0.22$ eV and the Gaussian broadening factor is $\sigma = 0.075$ eV. The shaded region around the main calculated absorption spectrum represents the error in $\varepsilon(\lambda)$ due to statistical sampling, as detailed in ref. 21.

nuclear wavefunctions and the possible limitations of the harmonic approximation for the Wigner distribution.[14,21,22,24] The description of low-frequency (anharmonic) normal modes of flexible molecules such as those considered in this work, may lead to artifacts in $\varepsilon(\lambda)$ if these modes are photoactive (see Section S5 in the SI for details).[24] These artifacts may be overcome when other sampling strategies such as *ab initio* molecular dynamics with a quantum thermostat are used for the ground-state distribution.[24]

We stress that selecting an appropriate electronic-structure method is crucial for accurately describing excited states of complex molecules while maintaining the low computational cost required by the NEA. For example, the absorption spectrum presented in Fig. 2d required 3000 single-point calculations (see Section S6 in the SI for details), which may limit the use of an accurate electronic-structure method to molecules composed of only a few dozen atoms. LR-TDDFT offers a good balance between efficiency and accuracy, although caution is advised before its use. For example, the transitions that contribute to the first two absorption bands in MCH^+ and SP exhibit a partial charge-transfer character (see Table S1), requiring long-range corrected hybrid functionals. A benchmark study (see Section S7) is therefore crucial to assess the performance of LR-TDDFT against wavefunction-based approaches.

Herein, we propose a pragmatic protocol combining conformer sampling and the NEA, deployed using freely-available computational tools, to predict reliable absorption spectra of relatively large photoacids used for seawater CO_2 capture and release in solution. The protocol focuses on describing the shape of the absorption bands and their absolute intensity, required to predict their overlap with a light source and as such the rate of the photophysical process of interest. This protocol can be transferred to study the light-absorption properties of other molecular species of interest in photocatalysis or solar technologies, offering an appealing intermediate strategy between single-point calculations and more advanced schemes.[25]

The authors thank Dr Richard Y. Liu for providing the experimental absorption spectra of MCH^+ and SP. The authors acknowledge EPSRC for funding this research through the Programme Grants EP/V026690/1 and EP/X026973/1. This work was carried out using the computational facilities of the Advanced Computing Research Centre, University of Bristol. FJH ackowledges the support from the School of Physical and Chemical Sciences at Queen Mary University of London and the support from the QMUL Research-IT.

Conflicts of interest

There are no conflicts to declare.

Data availability

Data supporting this publication can be obtained from the supplementary information (SI). Supplementary information is available. See DOI: **https://doi.org/10.1039/d5cc04069h**.

References

1 *Climate Change 2014: Mitigation of Climate Change – Working Group III Contribution to the Fifth Assessment Report of the Intergovernmental Panel on Climate Change*, 2014, **https://www.ipcc.ch/report/ar5/wg3/**.
2 V. Masson-Delmotte, P. Zhai, A. Pirani, S. L. Connors, C. Péan, Y. Chen, L. Goldfarb, M. I. Gomis, R. Matthews, S. Berger, M. Huang, O. Yelekçi, R. Yu, B. Zhou, E. Lonnoy, T. K. Maycock, T. Waterfield, K. Leitzell and N. Caud, *Climate Change 2021: The Physical Science Basis – Contribution of Working Group I to the Sixth Assessment Report of the Intergovernmental Panel on Climate Change*, 2021, **https://www.ipcc.ch/report/ar6/wg1/**.
3 U. I. Premadasa, V. Bocharova, A. R. Miles, D. Stamberga, S. Belony, V. S. Bryantsev, A. Elgattar, Y. Liao, J. T. Damron, M. K. Kidder, B. Doughty, R. Custelcean and Y.-Z. Ma, *Angew. Chem., Int. Ed.*, 2023, **62**, e202304957.
4 U. I. Premadasa, B. Doughty, R. Custelcean and Y.-Z. Ma, *ChemPlusChem*, 2024, **89**, e202300713.
5 A. M. Alfaraidi, B. Kudisch, N. Ni, J. Thomas, T. Y. George, K. Rajabimoghadam, H. J. Jiang, D. G. Nocera, M. J. Aziz and R. Y. Liu, *J. Am. Chem. Soc.*, 2023, **145**, 26720–26727.
6 P. Saha, J. Meeder, S. Singh, S. Ramesh, M. Nippe and D. G. Kwabi, *J. Phys. Chem. C*, 2024, **128**, 4914–4923.
7 A. de Vries, K. Goloviznina, M. Reiter, M. Salanne and M. R. Lukatskaya, *Chem. Mater.*, 2024, **36**, 1308–1317.
8 D. Cotton, T. Khuu, K. Takematsu, B. Delibas and J. M. Dawlaty, *J. Phys. Chem. Lett.*, 2024, **15**, 7782–7787.
9 O. Alghazwat, A. Elgattar and Y. Liao, *Photochem. Photobiol. Sci.*, 2023, **22**, 2573–2578.
10 H. Seo, J. Schretter, M. Massen-Hane and T. A. Hatton, *J. Am. Chem. Soc.*, 2024, **146**, 26777–26785.
11 R. E. Zeebe, *CO_2 in seawater: Equilibrium, kinetics, isotopes,* Elsevier Science & Technology, 2001.
12 Y. Liao, *Acc. Chem. Res.*, 2017, **50**, 1956–1964.
13 A. Prlj, L. M. Ibele, E. Marsili and B. F. E. Curchod, *J. Phys. Chem. Lett.*, 2020, **11**, 5418–5425.
14 A. Prlj, E. Marsili, L. Hutton, D. Hollas, D. Shchepanovska, D. R. Glowacki, P. Slavíček and B. F. E. Curchod, *ACS Earth Space Chem.*, 2022, **6**, 207–217.
15 S. Grimme, *J. Chem. Theory Comput.*, 2019, **15**, 2847–2862.
16 P. Pracht, F. Bohle and S. Grimme, *Phys. Chem. Chem. Phys.*, 2020, **22**, 7169–7192.
17 T. Yanai, D. P. Tew and N. C. Handy, *Chem. Phys. Lett.*, 2004, **393**, 51–57.
18 M. Garcia-Ratés and F. Neese, *J. Comput. Chem.*, 2019, **41**, 922–939.
19 M. J. Frisch, J. A. Pople and J. S. Binkley, *J. Chem. Phys.*, 1984, **80**, 3265–3269.
20 F. Neese, *Wiley Interdiscip. Rev.: Comput. Mol. Sci.*, 2022, **12**, e1606.
21 R. Crespo-Otero and M. Barbatti, *Theor. Chem. Acc.*, 2012, **131**, 1237.
22 R. Crespo-Otero and M. Barbatti, *Chem. Rev.*, 2018, **118**, 7026–7068.
23 M. Barbatti, M. Bondanza, R. Crespo-Otero, B. Demoulin, P. O. Dral, G. Granucci, F. Kossoski, H. Lischka, B. Mennucci, S. Mukherjee, M. Pederzoli, M. Persico, M. Pinheiro, Jr, J. Pittner, F. Plasser, E. Sangiogo Gil and L. Stojanovic, *J. Chem. Theory Comput.*, 2022, **18**, 6851–6865.
24 A. Prlj, D. Hollas and B. F. E. Curchod, *J. Phys. Chem. A*, 2023, **127**, 7400–7409.
25 A. Khanna, S. V. Shedge, T. J. Zuehlsdorff and C. M. Isborn, *J. Chem. Phys.*, 2024, **161**, 044121.